American Mineralogist, Volume 82, pages 1101–1110, 1997

Transformation of titanomagnetite to titanomaghemite: A slow, two-step, oxidation-ordering process in MORB

WEIXIN XU,[1] DONALD R. PEACOR,[1] WAYNE A. DOLLASE,[2] ROB VAN DER VOO,[1] AND RICK BEAUBOUEF[3,†]

[1]Department of Geological Sciences, University of Michigan, Ann Arbor, Michigan 48109-1063, U.S.A.
[2]Department of Earth and Space Sciences, University of California Los Angeles, Los Angeles, California 90095-1567, U.S.A.
[3]Department of Geosciences, University of Houston, Houston, Texas 77204-5503, U.S.A.

ABSTRACT

Magnetic iron oxides in a sequence of pillow basalts that were dredged from the Atlantic Ocean floor have been studied to characterize titanomaghemite and to define the processes of maghemitization. Distances from the spreading ridge and ages (in parentheses) of the samples are 0–10 (0–1), 160 (9), 450 (26), and 900 km (70 Ma).

Iron titanium oxides occur as 1 to 10 μm-sized dendritic and cruciform-shaped crystals with identical appearances in all samples and with no signs of change or significant heterogeneity in composition or structure as observed by TEM and AEM. Parameters change progressively from the youngest to the oldest, e.g., Curie temperature = 180 to 360 °C; lattice parameter = 8.466 to 8.361 Å; number of octahedral cations per cell from Rietveld refinement = 14.8 to 12.1; mean hyperfine (internal) fields at 300 K from Mössbauer data = 37 to 45 T. The large Ti contents (Uv_{60} to Uv_{70}) are nearly constant. SAED patterns show superstructure reflections only for the oldest sample.

The youngest sample has parameters corresponding to nearly unoxidized titanomagnetite, whereas the oldest is near-end-member titanomaghemite. Intermediate samples are partially altered but display no superstructure reflections, implying a lack of significant ordering of vacancies. The data therefore show that the process of (titano)maghemitization has two distinctly different components: (1) oxidation and loss of Fe, with creation of disordered vacancies, and (2) ordering of vacancies. The data collectively imply a process dominated by solid state diffusion of Fe from the crystals, oxidation of Fe, and creation of vacancies wherein the O closest-packed framework is preserved, in sharp contrast to a model of addition of O or to dissolution and neocrystallization.

INTRODUCTION

Magnetic minerals in ocean-floor basalts have been much studied because magnetic anomalies of oceanic crust have served as the primary data in our understanding of the evolution of oceanic lithosphere and of plate tectonics. Titanomagnetite [Fe_2TiO_4 (ulvöspinel)·Fe_3O_4 (magnetite), or $Fe_{(3-x)}Ti_xO_4$] is the principal magnetic mineral in unaltered ocean floor basalts, but it undergoes alteration to (titano)maghemite (Irving 1970; Ozima et al. 1974; Petersen et al. 1979; Smith 1987; Pariso and Johnson 1991). The transformation involves oxidation of ferrous iron and production of (ordered) cation vacancies. O'Reilly and Banerjee (1967) defined the degree of maghemitization by the oxidation parameter Z in the expression

$$Fe^{2+} + \frac{Z}{2}O \rightarrow Z\,Fe^{3+} + (1 - Z)\,Fe^{2+} + \frac{Z}{2}O^{2-}$$

where Z is the fraction of ferrous iron that has been oxidized to ferric iron, ranging from 0 to 1. The parameter Z can be estimated using the measured Curie temperature or cell parameter, provided the effects of solid solution of components such as Ti are known (Readman and O'Reilly 1972; Ozima et al. 1974; Nishitani and Kono 1983; Moskowitz 1987).

Maghemitization of primary titanomagnetite has been interpreted to be the main cause of decrease in NRM intensity with increasing age of MORB, concomitant with increasing distance from spreading ridges (Irving 1970; Marshall and Cox 1972; Bleil and Petersen 1983). An understanding of such relations requires characterization of the crystal chemistry of titanomaghemite, but because of the difficulties in obtaining pure natural material, studies since the 1960s have been largely restricted to synthetic titanomagnetite and titanomaghemite (e.g., O'Reilly and Banerjee 1967; Ozima and Sakamoto 1971;

* Present address: Department of Geology, Arizona State University, Tempe, AZ 85287-1404, U.S.A.
† Present address: Exxon Production Research Co., P.O. Box 2189, Houston, TX 77252-2189, U.S.A.

0003–004X/97/1112–1101$05.00

Readman and O'Reilly 1972; Nishitani and Kono 1982, 1983; Moskowitz 1987; Goss 1988). Natural materials have been less extensively studied (e.g., Marshall and Cox 1972; Petersen et al. 1979; Beske-Diehl 1990; Furuta 1993), in part because of their small grain size, which is generally less than approximately 5 μm. Consequently, the crystal-chemical properties of (titano)maghemite and intermediate products of maghemitization remain largely uncharacterized. It is especially important to determine the characteristics of intermediate products because they are the key to an understanding of the process of maghemitization.

Although it is well known that the magnetic properties of oxidized titanomagnetite are directly related to the maghemitization process (Bleil and Petersen 1983; O'Reilly 1983; Banerjee 1991), the alteration products and processes are incompletely defined. The transformation is generally inferred to occur by one of two very different processes: (1) loss of Fe relative to Ti, with the O closest-packed substructure being invariant (e.g., Petersen et al. 1979), or (2) addition of O with constant Fe: Ti ratio (e.g., Readman and O'Reilly 1972). The general concensus favors transformation by diffusion of Fe out of crystals (e.g., Furuta 1993, and references therein). Both mechanisms appear to involve solid state diffusion at relatively low temperatures and in the presence of a fluid in naturally occurring samples, as implied, for example, by retention of grain shapes (Petersen and Vali 1987) and of Ti contents (Furuta 1993). Transformation in laboratory experiments usually has been promoted by heating at high temperatures in air to promote oxidation (e.g., Readman and O'Reilly 1972; Moskowitz 1987; Fukasawa et al. 1993), and infrequently by heating in fluid (Ryall and Hall 1979; Kelso et al. 1991). Although heating in air presumably involves diffusion of Fe, it involves conditions that are unlike those in nature, whereas heating in H_2O may involve dissolution and neocrystallization rather than diffusion of Fe.

The reactant phase in marine basalts is dominantly titanomagnetite with an ulvöspinel component of approximately 0.62 (Bleil and Petersen 1977; Moskowitz and Banerjee 1981; Pariso and Johnson 1991). Titanomaghemite with ordered vacancies was found to retain primary Ti contents (Furuta 1993). However, little is known about the relation between composition and cation oxidation in samples with intermediate values of ordering, because such materials have not been well characterized. The ability of the oxidized products to retain components such as Ti is a key to the nature of the process, however, because Ti should be retained during solid state diffusion and lost during water-mediated dissolution and neocrystallization.

The specific vacancy distribution of natural titanomaghemite is not known. The detailed structure of maghemite seems process dependent (Waychunas 1991, and references therein), because at least three symmetries have been proposed for maghemite, including one corresponding to a face-centered cubic structure (Goss 1988), one with a tetragonal superlattice having $c = 3A$ (Boudeulle et al. 1983; Greaves 1983), and one with a primitive cubic superlattice (Smith 1979; Goss 1988; Banfield et al. 1994). A primitive cubic superlattice has been reported for naturally occurring titanomaghemite (Collyer et al. 1988; Smith 1979; Price and Putnis 1979), but the oxidized equivalent of titanomagnetite occurring in MORB remains unstudied.

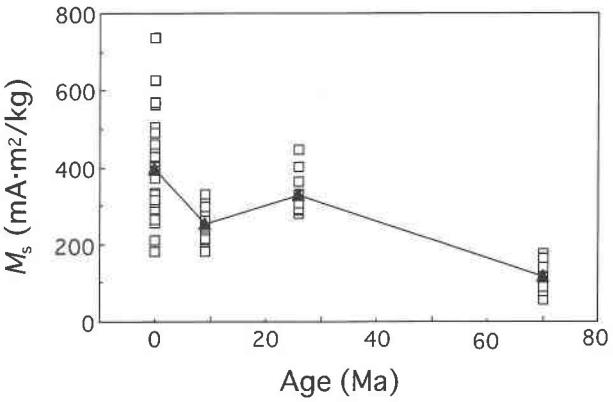

FIGURE 1. Plot of saturation magnetization (M_s) vs. age of bulk rock samples, showing decrease of M_s with increasing age.

To investigate the relationship between MORB magnetic properties and mineralogic properties, we studied a series of four pillow basalts from the Atlantic Ocean collected at increasing distances, and therefore increasing ages (<1 Ma to 70 Ma), from the mid-Atlantic Ridge (Beaubouef 1993; Xu et al. 1994). These samples are of interest because they display a systematic decrease in NRM with increasing age that was tentatively hypothesized to be related to the maghemitization process (Beaubouef 1993). Figure 1, plot of saturation magnetization vs. age, demonstrates decreasing magnetization with age. Xu et al. (1995) showed that the rock magnetic properties are not related entirely to titanomagnetite-titanomaghemite with grain sizes on the order of a micrometer that are easily observed and the source of past observations. Instead the magnetic properties are primarily related to changes in submicrometer-sized titanomagnetite found in interstitial glass. In this report, we characterize the common kind of titanomagnetite-titanomaghemite that occurs abundantly in MORB with grain sizes in the optical range. Because such material was incompletely characterized, in part because of its small grain size, this study emphasizes TEM and AEM observations, but also includes data from SEM, EMPA, XRD, Mössbauer analysis, and magnetic studies. These data are then used to show that the transformation of titanomagnetite to titanomaghemite in oceanic basalt involves two processes that may occur at different times, oxidation-cation-diffusion and ordering of resultant cation vacancies.

SAMPLE DESCRIPTION AND EXPERIMENTAL PROCEDURES

The samples were dredged from four sites at distances of <10, 160, 450, and 900 km from the mid-Atlantic

ridge and are referred to with corresponding site numbers one through four. All hand samples are pillow basalts, which grade from black in the youngest samples, through grey or dark brown, to brown or reddish brown in the oldest sample, as consistent with increasing degree of oxidation (see below). To ensure that the full range of textures was observed, thin sections were prepared from pillow rims as well as pillow interiors.

Thin sections were made with "sticky wax" as adhesive so that sections could first be studied by optical and SEM techniques, with selected areas subsequently removed and ion-milled for imaging by TEM. SEM observations were made with a Hitachi S-570 instrument fitted with back-scattered electron detector and Kevex Quantum EDS system. TEM and AEM data were obtained using a Philips CM-12 STEM fitted with a Kevex Quantum EDS system, with procedures as defined by Jiang et al. (1990).

To obtain concentrates of the magnetic phases for measurement of magnetic properties, Mossbauer spectra, and XRD patterns, one sample from each site was crushed in air to obtain grains <1 mm in size. These were then ground under acetone in a tungsten alloy mortar, and the magnetic fraction was separated using a REE magnet. The separates were subsequently found (see below) to contain approximately 18 to 35% magnetic phases. Further separation was not possible owing to the fine-grained nature of the intergrowths. Curie temperatures (T_c) and Mössbauer spectra were measured at the Institute for Rock Magnetism, University of Minnesota. The T_c values were obtained using an automated, vibrating sample magnetometer, by heating and cooling samples sealed in silver foil at a rate of 20 °C/min, in an applied field of 500 mT, both in helium and in air. These ^{57}Fe Mössbauer data were obtained as 1024-channel spectra, folded, and summed pairwise to yield 256-point spectra. The spectra were fitted with the program MOSFIT, a program developed at UCLA. Spectra were fitted with a magnetically split, six-line component, a paramagnetic Fe^{3+} doublet, and a paramagnetic Fe^{2+} doublet. Because of the variability or other complexities of the magnetic phases (see below) individual lines of the magnetic sextet were approximated by one to three subcomponents, but no significance was inferred for the individual subcomponents.

X-ray powder diffraction patterns were obtained using a Philips XRG 3100 diffractometer fitted with a graphite monochromator mounted near the receiving slit, Cu$K\alpha$ radiation (35 kV, 15 mA), and variable divergence slit. Scans were made from 15° to 75° 2θ with a step interval of 0.01° and count time of 6 s. Rietveld analysis was carried out with the program DBW (Wiles and Young 1981), with refinement of the usual pattern parameters (background, 2θ zero-point, peak width, and Gaussian-Lorentzian mix). No regions of the diffraction patterns were excluded. The separates contained significant amounts of pyroxene and plagioclase. Positional parameters of plagioclase (Toman and Frueh 1973), clinopyroxene (Peacor 1967), and orthopyroxene (Ghosc 1965) were held constant, but cell parameters and concentrations were refined. The magnetite-maghemite substructure parameters that were refined included subcell parameter (A), oxygen coordinate (u), and occupancy of the octahedral sites. The tetrahedral site was assumed to be occupied only by Fe, and all Ti was assumed to be in the octahedral site with the Fe/Ti ratio being held constant at a value separately determined for each sample by AEM. These assumptions regarding the site occupancies have previously been verified by several refinements of titanomagnetite or titanomaghemite structures (e.g., Collyer et al. 1988).

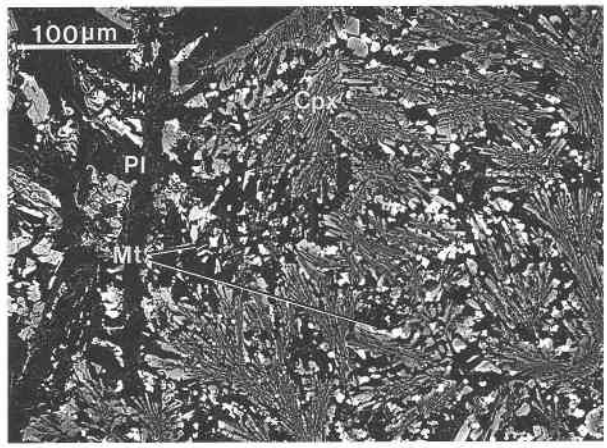

FIGURE 2. SEM backscattered electron image showing the typical texture of pillow basalt sample one with titanomagnetite commonly concentrated in areas between dendritic pyroxene aggregations. Platy dark grey area (Pl) = plagioclase lath; grey area (Cpx) = dendritic pyroxene aggregations; bright spots (Mt) = titanomagnetite; irregular dark grey area = interstitial glass.

DATA AND OBSERVATIONS

SEM observations of thin sections

The texture shown in Figure 2 is representative of all four samples, with the exception of the thin, glass-rich pillow rinds. All samples consist primarily of microphenocrysts of plagioclase and olivine within a fine-grained matrix of plagioclase, pyroxene, olivine, titanomagnetite, and residual glass. The dominant opaque mineral is euhedral titanomagnetite or titanomaghemite, occurring commonly with dendritic (Fig. 3a) and cruciform (Fig. 3b) shapes consistent with quenching from high temperatures (Somboonsuk and Trivedi 1985). Grain sizes that can be resolved by BSE imaging are dominantly in the range 1 to 10 μm. Qualitative EDS analyses are consistent with relatively high Ti concentrations that are approximately equal in all samples. There is limited variation in composition within a thin section, individual crystals having compositions varying by up to Uv_8 (as shown by AEM data; see below) from crystal cores to rims, but crystals are otherwise homogeneous.

STEM observations

Figure 4a is a low magnification, bright field image of typical magnetic material from sample four. The magnetic

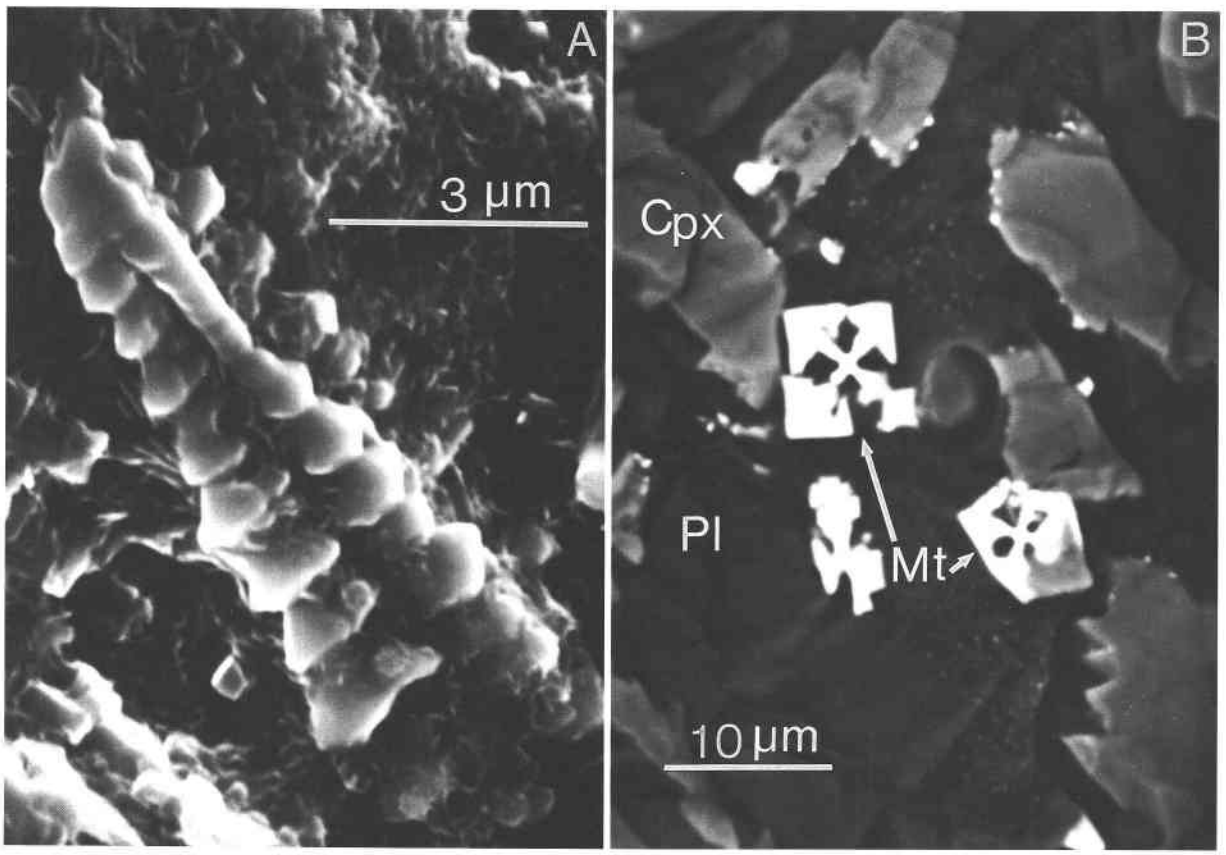

FIGURE 3. (A) SEM secondary electron image showing dendritic titanomagnetite in sample four. (B) SEM backscattered electron image showing cruciform titanomagnetite in sample one. Pl = plagioclase; Cpx = clinopyroxene; Mt = titanomagnetite.

phase has shapes identical to those in the other three samples and appears to be uniform in texture. There are no cracks that might arise because of decreases in lattice parameters as a result of maghemitization e.g., as observed by Petersen and Vali (1987). Figure 4b is a corresponding [010] zone axis selected area electron diffraction (SAED) pattern. It has strong substructure reflections (e.g., 202 and 400) characteristic of a phase with the spinel structure but also has weak superstructure reflections (e.g., 100) of a kind characteristic of maghemite. SAED patterns obtained from within a single micrometer-sized crystal were uniform in orientation and relatively sharp, implying that each grain is a well-formed, single crystal.

Superstructure reflections were observed in every crystal studied from sample four. They always were observed to have the same approximate intensities relative to the substructure reflections. By contrast, no superstructure reflections were observed in magnetic phases for samples one to three, even though SAED patterns were obtained on tens of crystals from several ion-milled samples from each locality.

The space group of a natural sample of titanomaghemite was determined by Collyer et al. (1988) to be $P4_132$ or $P4_332$, the cell having $a = 8.341$ Å, i.e., a cell with the same dimensions as that of magnetite, but with reflections in positions that violate F centering. Smith (1979) first suggested that maghemite satisfies those relations, and Banfield et al. (1994) made equivalent observations. However, Banfield et al. also observed that some of their material gave extra reflections that required doubling of the magnetite cell parameter. Boudeulle et al. (1983) and Greaves (1983) reported that synthetic maghemite can be tetragonal with a superlattice with $c = 3A$. The SAED patterns obtained in this study show superstructure reflections that only violate F centering and therefore are consistent with a cell with $a = A$. However, reflections of the type $h00$ with h odd are prominent and therefore inconsistent with space group $P4_132$ or its enantiomorph. The [100] SAED patterns of different crystals displayed fourfold symmetry in all cases, with reflections of equivalent indices having equivalent intensities as visually estimated. Such relations are consistent with cubic symmetry or of unit-cell twinning of a symmetry with a noncubic space group. Our data do not permit a direct identification of space group. However, imaging under various conditions, including attempts to image possible antiphase domains by dark-field imaging with superstructure reflections, failed to detect further textural relations.

Some representative AEM analytical data are listed in

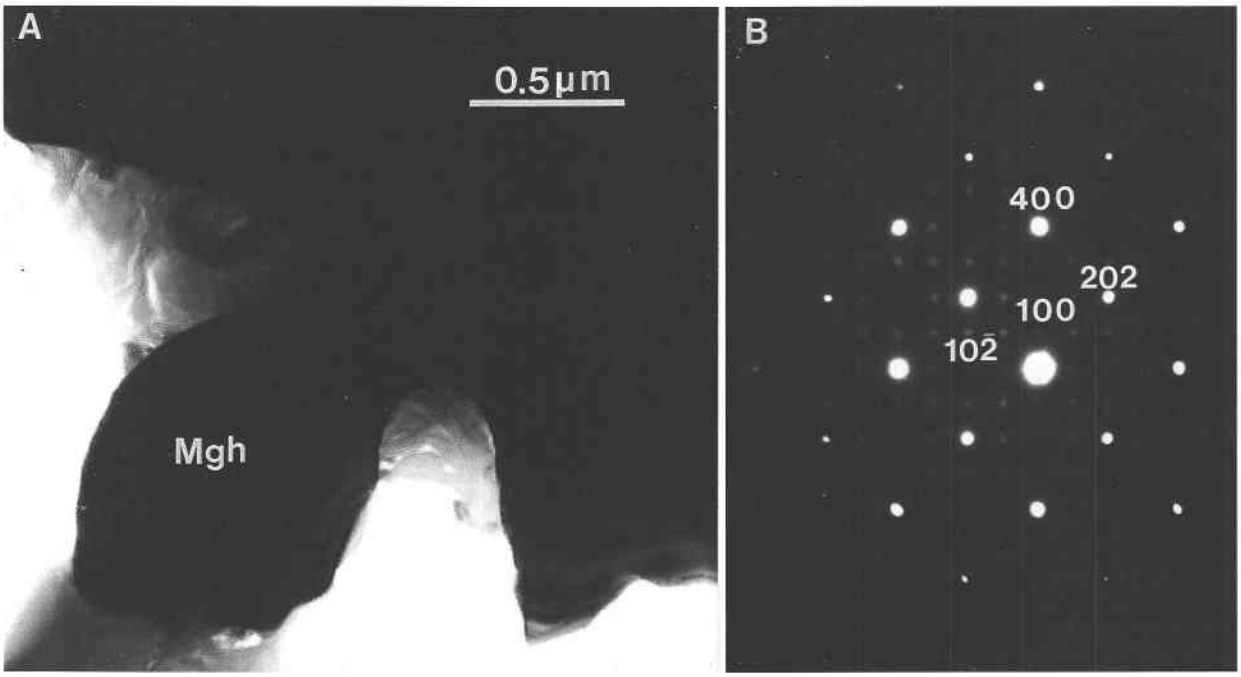

FIGURE 4. (A) TEM bright field image of titanomaghemite (Mgh) from sample four, showing that it has the original cruciform texture. (B) Electron diffraction pattern of the titanomaghemite of the same sample as in (A), showing that it has the diffraction pattern of a primitive cubic superlattice (100), which is distinct from that of the face-centered cubic lattice.

Table 1. Although there are differences in composition between materials from different localities, the range in composition was found to be narrow for any one sample, with only relatively small concentration gradients from core to rim; e.g., Figure 5 shows a gradient corresponding to an increase in the Ti/Fe ratio from 0.23 to 0.27 from core to rim, a relative change typical of all samples. The calculated average ulvöspinel components for each sample vary from $x = 0.58$ to $x = 0.73$, but there is no trend in composition with distance from the spreading ridge. Indeed, sample four has the highest ulvöspinel component, implying that there has been no significant loss of Ti. In addition, the small core-to-rim concentration gradients present in younger samples also occur in the oldest samples.

A second mode of titanomagnetite-titanomaghemite

TABLE 1. Selected typical AEM analyses of titanomagnetite in studied samples of pillow basalts from mid-Atlantic Ocean*

Oxide (wt%)	Sample 1		Sample 2		Sample 3		Sample 4	
Al_2O_3	0.00	1.04	1.90	1.63	0.96	0.54	2.86	1.96
SiO_2	1.10	0.00	0.68	0.79	0.00	0.00	0.00	0.95
CaO	0.60	0.70	0.53	0.69	0.00	0.00	0.93	0.51
TiO_2	20.71	20.16	22.17	22.98	19.58	19.27	22.87	24.74
MnO	0.73	2.02	1.46	1.15	1.23	1.44	0.96	0.72
Fe_2O_3	76.38	76.08	73.26	72.76	76.95	77.85	72.36	71.11
Total†	100.00	100.00	100.00	100.00	100.00	100.00	100.00	100.00
Number of cations calculated on the basis of four O atoms								
Al	0.000	0.042	0.073	0.063	0.063	0.021	0.110	0.075
Si	0.039	0.000	0.022	0.026	0.000	0.000	0.000	0.030
Ca	0.021	0.025	0.019	0.024	0.000	0.000	0.032	0.018
Ti	0.518	0.507	0.544	0.563	0.487	0.481	0.560	0.600
Mn	0.021	0.057	0.040	0.032	0.034	0.040	0.026	0.020
Fe	1.910	1.916	1.799	1.783	1.915	1.947	1.771	1.726
Total	2.509	2.545	2.498	2.489	2.537	2.535	2.500	2.469
Ti/Fe	0.271	0.265	0.313	0.316	0.254	0.247	0.316	0.347
x‡	0.640	0.666	0.715	0.720	0.608	0.594	0.681	0.743

* Two columns for each sample represent two different analyses.
† Oxide wt% normalized to 100%.
‡ x represents the ulvöspinel component in $Fe_{1-x}Fe_2Ti_xO_4$ and is calculated from Ti/Fe ratios $x = 3Ti/(Ti + Fe)$.

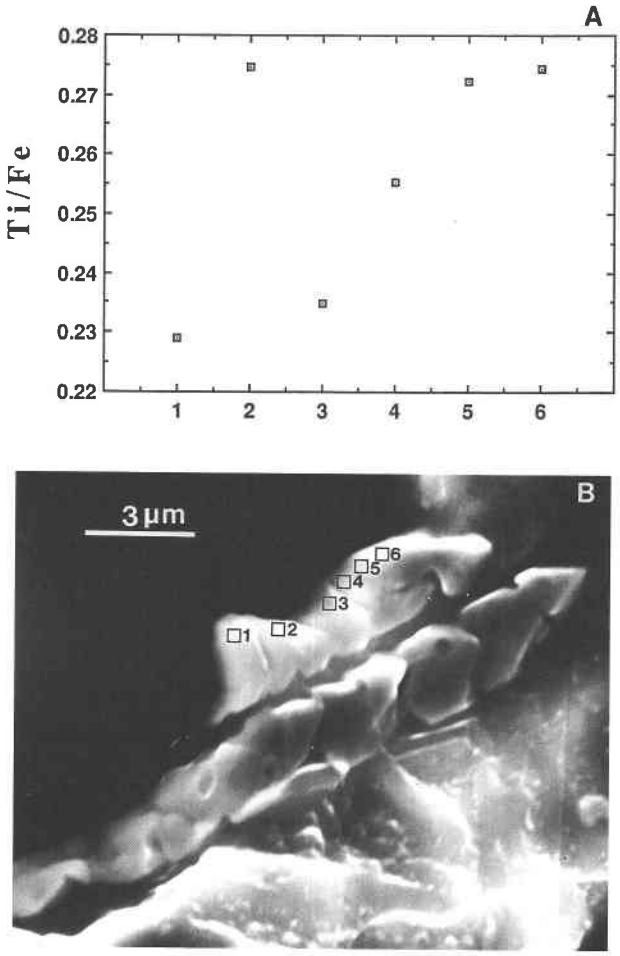

FIGURE 5. (A) Compositional zoning within dendritic titanomagnetite, with numbers corresponding to AEM analyses for which areas are shown in Figure 5B. (B) SEM secondary electron image of sample one, showing a cross-section of one dendritic titanomagnetite and areas of AEM analysis.

occurrence is as single domain-sized (approximately 200 Å) crystals within residual glass (Xu et al. 1995). Although important as a carrier of the NRM, it accounts for $\ll$ 10% of the magnetic material, and therefore it does not contribute significantly to the properties described in this study.

X-ray diffraction data

No superstructure reflections were observed by powder XRD from any sample, including sample four for which superstructure reflections were observed in SAED patterns (Fig. 4b). Powder X-ray diffraction patterns of synthetic maghemite (e.g., γ-Fe_2O_3 of Pfizer Chemical Co.), with completely ordered octahedrally coordinated cations and vacancies, clearly show weak superstructure reflections. The intensity of such reflections is maximized for both maximum oxidation and cation-vacancy ordering. Because samples two through four are largely to completely oxidized, these relationships imply that ordering must be incomplete.

Individual R_{Bragg} factors for the Rietveld refinement are good especially for the magnetic phases, ranging from 2.4 to 4.3%. Structure parameters of the magnetic phases are listed in Table 2, along with values obtained by others for refinements of well-characterized magnetic phases with the spinel structure. Extensive data on the cell size of the ulvöspinel-magnetite ($0 < x < 1$; $Z = 0$) and magnetite-maghemite ($x = 0$; $0 < Z < 1$) solid solutions (e.g., Lindsley 1976; Fukasawa et al. 1993; Senderov et al. 1993) show that A increases with increasing Ti content and decreases with increasing proportion of vacancies. The variation of lattice parameter away from those joins ($x = 0$ and $Z = 0$) is more complex and is discussed in detail by Xu et al. (1996). Here we note that from sample one to sample four the lattice parameters decrease from $a = 8.466$ (F-centered cell) to 8.361 Å (cell with reflections violating F centering). When corrected for the Ti contents measured by AEM and assuming linear relations between the lattice parameters, Ti contents, and vacancy contents, those values correspond closely to values for end-member unoxidized titanomagnetite (8.475 Å) and completely oxidized titanomaghemite (8.340 Å).

Proportions of components other than Fe and Ti were shown by AEM to be small (<1 wt%). Using relations for lattice parameter variation as a function of concentration of cations such as Mn and Al (Fukasawa el al. 1993), the small cation proportions were found, collectively, to

TABLE 2. Rietveld-refined spinel structure parameters

Sample	A (Å)	u	oct/cell	References
No. 1	8.466(2)	0.2625(21)	14.82(29)	This paper
No. 2	8.402(1)	0.2583(20)	13.97(22)	This paper
No. 3	8.381(3)	0.2534(55)	14.06(53)	This paper
No. 4	8.361(1)	0.2545(36)	12.10(31)	This paper
Ti-Mh	8.341(1)	0.2554*	13.1	Collyer et al. (1988)
γ-Fe_2O_3	8.3515(5)	0.2579*	(13.3)	Dollase (unpublished)
γ-Fe_2O_3	8.341	—	(13.3)	Fukasawa et al. (1993)
γ-Fe_2O_3	8.3396	0.2551*	(13.3)	Greaves (1983)
Fe_3O_4	8.3970(1)	0.2550	(16)	O'Neill & Dollase (1994)
Fe_2TiO_4	8.536(1)	0.265(10)	(16)	Lindsley (1976)

Note: oct/cell = number of Fe-occupied octahedra per unit cell.
* Refers to equivalent oxygen u-coordinate in space group $Fd3m$.

TABLE 3. Estimated spinel composition based on Rietveld refinement of XRD data

	Compositions estimated from cell dimensions						Compositions estimated from site occupancies					
Sample	Fe^{2+}	Fe^{3+}	Ti	Vacancy	O	*A* (Å)	Fe^{2+}	Fe^{3+}	Ti	Vacancy	O	R_{Bragg} (%)
No. 1	1.397	0.903	0.624	0.076	4	8.4664(11)	1.167	1.077	0.608	0.148	4	2.39
No. 2	0.658	1.351	0.658	0.333	4	8.4028(14)	0.789	1.251	0.668	0.292	4	2.43
No. 3	0.478	0.642	0.530	0.350	4	8.3828(35)	0.684	1.487	0.543	0.286	4	4.31
No. 4	0.211	1.716	0.608	0.465	4	8.3607(13)	0.201	1.723	0.607	0.469	4	3.00

have a negligible effect (<0.003 Å) on lattice parameters. Therefore, assuming that the lattice parameters are related linearly to the proportion of vacancies and Ti contents, compositions can be predicted as listed for each sample in Table 3. The compositions obtained from refined occupancies, calculated assuming full occupancy of the tetrahedral sites, are also given.

The proportions of vacancies determined by Rietveld refinement (Table 3) increase in a regular way from sample one to four. Likewise, the compositions calculated independently and on the basis of relations between the composition and refined vacancies and of composition and lattice parameters, are in good agreement.

Curie temperatures (T_c)

Table 4 shows that the measured Curie temperatures for the powdered, magnetic-concentrate samples increase from 180 to 350 °C, with increasing distance of samples from the spreading ridge. The Curie temperature of end-member magnetite (573 °C) has been shown to decrease with increasing ulvöspinel content and increase with increasing oxidation parameter, *Z* (Readman and O'Reilly 1972; Nishitani and Kono 1983; Moskowitz 1987). Using the AEM data of this study and the relationship between Ti content and T_c of Readman and O'Reilly (1972) and Nishitani and Kono (1983), Curie temperatures between 0 and 220 °C are predicted for samples one through four, assuming no oxidation. Those values are significantly smaller than the measured values, except for sample one. Other data imply little oxidation for sample one, but the differences in samples two through four can be attributed to maghemitization. Using the relationships developed by Readman and O'Reilly (1972), oxidation parameters were estimated to vary from 0.1 to 0.9 for samples one through four, in good agreement with other estimates.

TABLE 4. Measured and estimated T_c

Sample	Measured *x*	Reversibility*	Measured T_c (°C)	Estimated T_c (°C)† R-O	Estimated T_c (°C)† N-K
No. 1	0.64	yes	180	80–150	95–180
No. 2	0.74	no	260	20–80	0–95
No. 3	0.60	no	300	110–200	120–220
No. 4	0.72	no	350	40–100	20–100

* Reversibility of the thermal curve measured in helium.

† T_c estimated based on measured *x* values and Readman and O'Reilly's (R-O) (1972) and Nishitani and Kono's (N-K) (1983) contour diagrams, assuming $Z = 0$.

Mössbauer data

The Mössbauer spectra shown in Figure 6 are compared with spectra of pure maghemite and pure magnetite (Pankhurst and Pollard 1993). Parameters obtained from the spectra are listed in Table 5. All spectra are characterized by relatively broad peaks, but peaks become progressively sharper from sample one through sample four. Broadening is, in general, caused by chemical heterogeneity and small grain sizes. The titanomagnetite that occurs with grain sizes on the order of hundreds of angstroms in interstitial glass is lost through alteration as distance from the spreading ridge increases (Xu et al. 1995). The increase in sharpness of peaks with increasing distance therefore may be caused, at least in part, by loss of that fine-grained material.

The values of the isomer shift (Table 5) range from 0.31 to 0.35 mm/s. They are close to the value of 0.3 mm/s expected for octahedral Fe^{3+} (Collyer et al. 1988) but are very different from the value of 0.67 mm/s for pure magnetite with 50% Fe^{2+} in octahedral sites. Because the peaks of spectra from samples close to the ridge are extremely broad, the measured isomer shifts are inaccurate. Furthermore, in samples one and two, the isomer shifts listed in Table 5 refer only to the most prominent and readily identifiable component of the broad spectra. Because the spectra sharpen with degree of oxidation, focusing on that most prominent component emphasizes only the most oxidized component. Thus sample one, especially, may have a large Fe^{2+} component. Isomer shifts of the more sharpened spectra of samples three and four, at least, imply that most of the Fe is present as Fe^{3+}, however. The mean hyperfine (internal) fields at 300 K increase from sample one (37.0 T) to sample four (45.2 T), consistent with increasing proportion of Fe^{3+}.

DISCUSSION

Characterization of magnetic minerals

All data from sample one through sample four are consistent with progressive maghemitization with increasing distance from the spreading ridge, i.e., with increasing age. Sample one is unaltered or nearly unaltered titanomagnetite as indicated by the following relations: (1) The lattice parameter, *a*, corresponds to a total of 2.92 (octahedral plus tetrahedral) cations per four O atoms when adjusted for the measured Ti content, in comparison with the ideal value of 3 for unoxidized titanomagnetite. (2) The composition calculated on the basis of refined

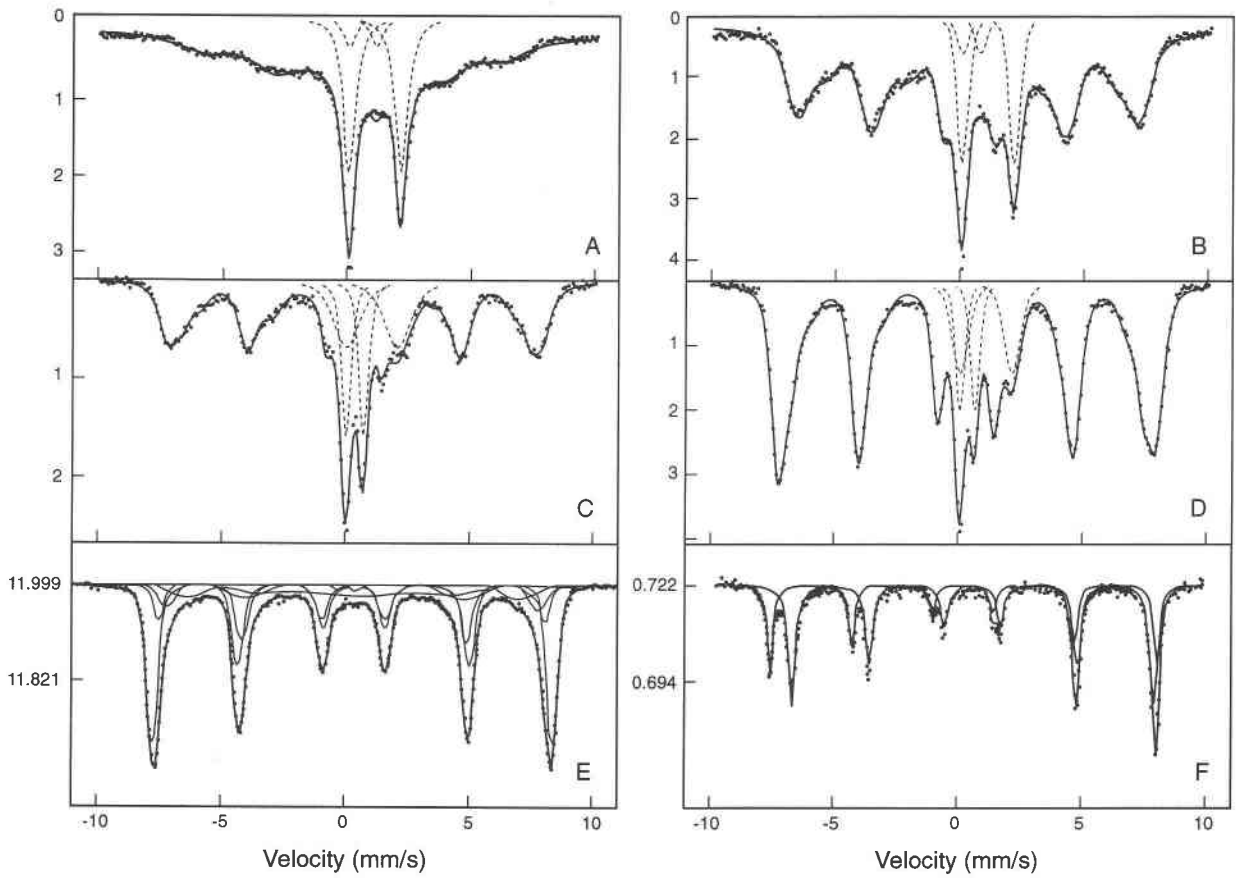

FIGURE 6. Mössbauer spectra of: **(A)** magnetic separates from basalt sample one; **(B)** magnetic separates from basalt sample two; **(C)** magnetic separates from basalt sample three; **(D)** magnetic separates from basalt sample four; **(E)** pure maghemite; and **(F)** pure magnetite. Spectra **A, B, C, D,** and **E** were measured at room temperature, whereas spectrum **F** was measured at 200 K. Spectra **E** and **F** are used by permission of Plenum Publishing Corp., from Pankhurst and Pollard (1993).

site occupancies has a total of 2.85 cations per four O atoms, consistent with a small amount of oxidation. (3) The O coordinate, $u = 0.2625$, is compatible with a non-oxidized phase with significant Ti but is considerably larger than that (0.255) predicted for titanomaghemite (with the specific Ti content measured by AEM). (4) The Curie temperature (180 °C) compares well with the predicted range of values (80–180 °C) for unoxidized titanomagnetite with the composition measured by AEM. (5) The thermal curve in He (magnetization vs. temperature) is reversible (Ozima and Ozima 1971; O'Reilly 1983).

By contrast with sample one, sample four is dominated by titanomaghemite that is nearly fully oxidized, as shown by: (1) The lattice parameter, A, has a value consistent with 0.21 Fe^{2+} and a total of 2.54 (tetrahedral and octahedral) cations per four O atoms. (2) The composition determined from the site occupancy data has 0.20 Fe^{2+}. There is a total of 2.53 cations per four O atoms. (3) The O coordinate, $u = 0.2545$, is compatible with nearly complete oxidation. (4) The Mössbauer pattern is compatible with complete or nearly complete oxidation of Fe. (5) The Curie temperature (350 °C) compares well with that predicted (350–450 °C) for oxidation parameter $Z = 0.9$ (Readman and O'Reilley 1972; Nishitani and Kono 1983). (6) The thermal curves in He are irreversible (Ozima and Ozima 1971; O'Reilly 1983). (7) The SAED patterns of all material that was observed showed superstructure reflections consistent with ordered vacancies. However, superstructure reflections were not observed in XRD patterns, whereas many authors have shown that XRD patterns of end-member, fully ordered maghemite show well-defined superstructure reflections. The intensities of such reflections are a function of both the proportions of vacancies and the degree of vacancy-cation

TABLE 5. Mean hyperfine (internal) fields at 300 K

Sample	H_0 (T)	I.S.*	%Fe†	Misfit (%)‡
No. 1	≈37	≈0.35	78	0.26
No. 2	≈40	≈0.35	84	0.31
No. 3	44.3	0.34	54	0.56
No. 4	45.2	0.31	76	0.25

* I.S. = Isomer (chemical) shift in mm/s relative to Fe metal.
† %Fe = Percent of total Fe in magnetic phase(s).
‡ Misfit = Percent of spectrum remaining unfitted.

order. The relative weakness of such reflections may therefore be due to incomplete ordering, given the near-end-member state of oxidation and therefore the high proportion of vacancies, even taking into consideration the smaller proportion of vacancies relative to Ti-free maghemite.

Intermediate samples two and three have lattice parameters, O coordinates, cation site occupancies, and parameters of Mössbauer patterns that are intermediate to those of samples one and four. For example, compositions determined from lattice parameters or octahedral site occupancies have octahedral plus tetrahedral cation totals in the range 2.65 to 2.71, in comparison with the ideal value of 3 for unoxidized material. Those parameters therefore demonstrate that samples two and three have intermediate states of maghemitization. However, the spinel phases give SAED patterns that, despite overexposure of photographs, fail to show any superstructure reflections, implying that the vacancies are not ordered or at most are only partially ordered.

Transformation mechanism

It is generally believed that the transformation of titanomagnetite to titanomaghemite occurs by oxidation of Fe, with solid-state diffusion of Fe to crystal boundaries and thence to pore fluids rather than by addition of O. Perhaps the most compelling evidence for a process involving loss of Fe is the electron microprobe data of Furuta (1993) who showed that the average Ti/O ratio of titanomaghemite is unchanged relative to titanomagnemite, whereas the Ti/Fe ratio is diminished. Data of this study are consistent with such a process, including retention of crystal morphologies and the three-dimensional translational periodicity of the O atom array of the primary, igneous, single crystals, as indicated by SAED patterns. The differences in Ti/Fe ratios vary randomly over the range of samples studied as a function of oxidation state, apparently in part as a function of primary igneous compositions. They are therefore not definitive in supporting a process of loss of Fe; nevertheless, the sample with the largest Ti/Fe ratio and one that is significantly larger than that of unaltered MORB (0.25; Furuta 1993) is the most oxidized (sample four). The retention of subtle zoning from cores to rims in oxidized crystals implies minimal disruption in structure and composition, however. A process of diffusion and loss of small Fe cations is one that maintains the integrity of the O closest-packed array, presumably by a process of cation-vacancy hopping. Although the effect of O diffusion into the structure cannot be directly assessed, it must involve at least local disruption in the anion array, and the occurrence of such a process is unlikely given the preservation of subtle features such as core-to-rim zoning. We therefore conclude that the data of this and other studies are conclusive with respect to a process of Fe diffusion from crystals concomitant with oxidation rather than with addition of O. In addition, the data are entirely inconsistent with a process of dissolution and neocrystallization of the micrometer-sized oxides; such a process generally leads to more stable materials, but Ti-rich titanomagnetite and vacancy-rich spinels such as maghemite are inherently metastable, implying the same for titanomaghemite.

Regardless of whether or not the process involves diffusion of Fe out of crystals or of O in, the data of this study show that it is one in which oxidation of Fe with creation of vacancies through loss of Fe is only a first step, before long-range ordering of vacancies. The absence of superstructure refections in the partially oxidized, intermediate samples of this study demonstrates that ordering occurs after oxidation and hence is at least in part a separate process. Likewise, the nearly complete state of oxidation of sample four, in conjunction with superstructure reflections that are weak in comparison with those of well-ordered structures, also implies that oxidation and creation of vacancies occurs before ordering. We therefore propose that the transformation of titanomagnetite to titanomaghemite may involve two processes, with oxidation and diffusion occurring first, at least in part independent of vacancy ordering. Ordering of vacancies and cations on octahedral sites occurs subsequently. The slow rates of solid state diffusion favor such a progressive sequence, in contrast to the more step-like functions that reflect dissolution and neocrystallization.

As noted above, maghemite and processes of maghemitization have been studied extensively in laboratory syntheses. Most experiments involve heating and oxidation in air, a process that presumably is based on the addition of O. Some experiments involve heating in fluids at high temperatures, conditions that favor dissolution and crystallization. Although the end-member phases may be readily synthesized by such methods, the data of this paper imply that the processes by which phases form in such laboratory experiments and in nature may be very different. Not only the composition, but the state of order and degree of homogeneity of synthetic materials must be identical to natural phases if the properties of synthetic materials are to be used as analogues of natural materials. Caution should therefore be used when synthetic phases are treated as analogous to naturally occurring magnetic oxides.

Acknowledgments

We thank B. Moskowitz and B.R. Frost who provided helpful comments on a previous draft of this paper and P. Solheid who collected Mössbauer data. The manuscript was also substantially improved by the suggestions of two anonymous reviewers. Research was supported by National Science Foundation (grant no. EAR 93-15913) and a visiting scholarship from the Institute for Rock Magnetism (IRM). The IRM is funded by grants from the Keck and National Science Foundation and the University of Minnesota.

References cited

Banerjee, S.K. (1991) Magnetic properties of Fe-Ti oxides. In Mineralogical Society of America Reviews in Mineralogy, 25, 107–128.

Banfield, J.F., Wasilewski, P.J., and Veblen, D.R. (1994) TEM study of relationships between the microstructures and magnetic properties of strongly magnetized magnetite and maghemite. American Mineralogist, 79, 654–667.

Beaubouef, R.T. Jr. (1993) Three case studies in the application of paleomagnetic and rock magnetic techniques to geologic problems: 1. 15° 20′ fracture zone, Atlantic Ocean, 2. Tauride Mountains, southern Turkey, and 3. Port au Port Peninsula, western Newfoundland, 287 p. Ph.D. thesis, University of Houston, Houston, Texas.

Beske-Diehl, S.J. (1990) Magnetization during low-temperature oxidation of seafloor basalts: no large scale chemical remagnetization. Journal of Geophysical Research, 95, 21,413–21,432.

Bleil, U. and Petersen, N. (1977) Magnetic properties of basement rocks, Leg 37, Site 332. In Initial Reports DSDP, 37, Washington, 446–456.

——— (1983) Variation in magnetization intensity and low-temperature titanomagnetite oxidation of ocean floor basalts. Nature, 301, 384–388.

Boudeulle, M., Batis-Landoulsi, H., Leclercq, C.-H., and Vergnon, P. (1983) Structure of γ-Fe_2O_3 microcrystals: vacancy distribution and structure. Journal of Solid State Chemistry, 48, 21–32.

Collyer, S., Grimes, N.W., Vaughan, D.J., and Longworth, G. (1988) Studies of the crystal structure and crystal chemistry of titanomaghemite. American Mineralogist, 73, 153–160.

Fukasawa, T., Iwatsuki, M., and Furukawa, M. (1993) State analysis and relationship between lattice constants and compositions including minor elements of synthetic magnetite and maghemite. Analytica Chimica Acta, 281, 413–419.

Furuta, T. (1993) Magnetic properties and ferromagnetic mineralogy of oceanic basalts. Geophysical Journal International, 113, 95–114.

Ghose, S. (1965) Mg^{2+}-Fe^{2+} order in an orthopyroxene, $Mg_{0.93}Fe_{1.07}Si_2O_6$. Zeitschrift Für Kristallographie, Kristallgeometrie, Kristallphysik, Kristallchemie, 122, 81–99.

Goss, C.J (1988) Saturation magnetization, coercivity and lattice parameter changes in the system Fe_3O_4-γFe_2O_3, and their relationship to structure. Physics and Chemistry of Minerals, 16, 164–171.

Greaves, C. (1983) A powder neutron diffraction investigation of vacancy ordering and covalence in γ-Fe_2O_3. Journal of Solid State Chemistry, 49, 325–333.

Irving, E. (1970) The mid-Atlantic ridge at 45° N XIV. Oxidation and magnetic properties of basalt: Review and discussion. Canadian Journal of Earth Sciences, 7, 1528–153.

Jiang, W.-T., Peacor, D.R., Merriman, R.J., and Roberts, B. (1990) Transmission and analytical electron microscopic study of mixed-layer illite/smectite formed as an apparent replacement product of diagenetic illite. Clays and Clay Minerals, 38, 449–468.

Lindsley, D.H. (1976) The crystal chemistry and structure of oxide minerals as exemplified by the Fe-Ti oxides. In Mineralogical Society of America Reviews in Mineralogy, 3, L1–L88.

Kelso, P.R., Banerjee, S.K., and Worm, H-U. (1991) The effect of low-temperature hydrothermal alteration on the remanent magnetization of synthetic titanomagnetites: A case for acquisition of chemical remanent magnetization. Journal of Geophysical Research, 96, 19,545–19,553.

Marshall, M. and Cox, A. (1972) Magnetic changes in pillow basalt due to sea floor weathering. Journal of Geophysical Research, 77, 6459–6469.

Moskowitz, B.M. (1987) Towards resolving the inconsistencies in characteristic physical properties of synthetic titanomaghemites. Physics of the Earth and Planetary Interiors, 46, 173–183.

Moskowitz, B.M. and Banerjee, S.K. (1981) A comparison of the magnetic properties of synthetic titanomaghemites and some oceanic basalts. Journal of Geophysical Research, 86, 11,869–11,882.

Nishitani, T. and Kono, M. (1982) Grain size effects on the low-temperature oxidation of titanomagnetite. Journal of Geophysics, 50, 137–142.

——— (1983) Curie temperature and lattice constant of oxidized titanomagnetite. Geophysical Journal of the Royal Astronomical Society, 74, 585–600.

O'Neill, H.St.C. and Dollase, W.A. (1994) Crystal structures and cation distributions in simple spinels from powder XRD structural refinements; $MgCr_2O_4$, $ZrCr_2O_4$, Fe_3O_4, and the temperature dependence of the cation distribution in $ZnAl_2O_4$. Physics and Chemistry of Minerals, 20, 541–555.

O'Reilly, W. (1983) The identification of titanomagnetites: Model mechanisms for the maghemitization and inversion process and their magnetic consequences. Physics of the Earth and Planetary Interiors, 31, 65–76.

O'Reilly, W. and Banerjee, S.K. (1967) The mechanism of oxidation in titanomagnetites: A magnetic study. Mineralogical Magazine, 36, 29–37.

Ozima, M. and Ozima, M. (1971) Characteristic thermomagnetic curve in submarine basalts. Journal of Geophysical Research, 76, 2051–2056.

Ozima, M. and Sakamoto, N. (1971) Magnetic properties of synthesized titanomaghemite. Journal of Geophysical Research, 76, 7035–7046.

Ozima, M., Joshima, M., and Kinoshita, H. (1974) Magnetic properties of submarine basalts and the implications on the structure of the oceanic crust. Journal of Geomagnetism and Geoelectricity, 26, 335–354.

Pankhurst, Q.A. and Pollard, R.J. (1993) Applied field Mössbauer spectroscopy of magnetic powders. In G.J. Long and F.G. GrandJean, Eds., Mössbauer spectroscopy applied to magnetism and material science, vol. 1, p. 77–113. Plenum Press, New York.

Pariso, J.E. and Johnson, H.P. (1991) Alteration processes at deep sea drilling project/ocean drilling program hole 504B at the Costa Rica rift: Implications for magnetization of oceanic crust. Journal of Geophysical Research, 96B, 11,703–11,722.

Peacor, D.R. (1967) Refinement of the crystal structure of pyroxene of formula $M_IM_{II}(Si_{1.5}Al_{0.5})O_6$. American Mineralogist, 138, 337–342.

Petersen, N. and Vali, H. (1987) Observation of shrinkage cracks in ocean floor titanomagnetite. Physics of Earth and Planetary Interiors, 46, 197–205.

Petersen, N., Eisenach, P., and Bleil, U. (1979) Low temperature alteration of the magnetic minerals in ocean floor basalts. In C.G.A. Harrison, M. Talwani, and D. Hayes, Eds., Deep drilling results in the Atlantic ocean: Ocean crust, 2, p. 169–209. American Geophysical Union, Washington, DC.

Price, G.D. and Putnis, A. (1979) Oxidation phenomena in pleonaste bearing titanomagnetites. Contributions to Mineralogy and Petrology, 69, 355–159.

Readman, P.W. and O'Reilly, W. (1972) Magnetic properties of oxidized (cation-deficient) titanomagnetites $(Fe,Ti,\square)_3O_4$. Journal of Geomagnetism and Geoelectricity, 69–90.

Ryall, R.J.C. and Hall, J.M. (1979) Laboratory alteration of titanomagneites in submarine pillow lavas. Canadian Journal of Earth Science, 16, 496–504.

Senderov, E., Dogan, A.U., and Navrotsky, E. (1993) Nonstoichiometry of magnetite-ulvöspinel solid solutions quenched from 1300 °C. American Mineralogist, 78, 565–573.

Smith, B.M. (1987) Consequences of the maghemitization on the magnetic properties of submarine basalts: Synthesis of previous works and results concerning basement rocks from mainly D.S.D.P. Legs 51 and 52, Physics of the Earth and Planetary Interiors, 46, 206–226.

Smith, P.P.K. (1979) The observation of enantiomorphous domains in a natural maghemite. Contributions to Mineralogy and Petrology, 69, 249–254.

Somboonsuk, K. and Trivedi, R. (1985) Dynamical studies of dendritic growth. Acta Metallurgica, 33, 1051–1060.

Toman, K. and Frueh, A.J. (1973) On the centrosymmetry of intermediate plagioclases. Zeitschrift Fuer Kristallographie, Kristallgeometrie, Kristallphysik, Kristallchemie, 138, 337–342.

Waychunas, G.A. (1991) Crystal chemistry of oxides and oxyhydroxides. In Mineralogical Society of America Reviews in Mineralogy, 25, 11–68.

Wiles, D.B. and Young, R. (1981) A new computer program for Rietveld analysis of X-Ray powder diffraction patterns. Journal of Applied Crystallography, 14, 149–151.

Xu, W., Van der Voo, R., Peacor, D.R., and Beaubouef, R. (1994) Maghemitization of titanomagnetite in dredged pillow basalts from the Atlantic ocean (abs.). Eos, 75, S126.

Xu, W., Peacor, D.R., Van der Voo, R., Dollase, W.A., and Beaubouef, R. (1995) Alteration of fine-grained titanomagnetite in the interstitial glass of pillow basalts from the Atlantic ocean: A component of the decrease in NRM intensity with aging (abs.). Eos, 76, S99.

——— (1996) Modified lattice parameter/Curie temperature diagrams for titanomagnetite/titanomaghemite within the quadrilateral Fe_3O_4-Fe_2TiO_4-Fe_2O_3-Fe_2TiO_5. Geophysical Research Letters, 23, 2811–2814.

Manuscript received December 9, 1996
Manuscript accepted July 30, 1997